Resonant Measurement of Nonreorientable Spin-Orbit Torque from a Ferromagnetic Source Layer Accounting for Dynamic Spin Pumping

Joseph A. Mittelstaedt and Daniel C. Ralph

Phys. Rev. Applied **16**, 024035 — Published 20 August 2021

DOI: 10.1103/PhysRevApplied.16.024035

Resonant Measurement of Non-Reorientable Spin-Orbit Torque from a Ferromagnetic Source Layer Accounting for Dynamic Spin Pumping

Joseph A. Mittelstaedt[1] and Daniel C. Ralph[1, 2]
[1] *Cornell University, Ithaca, NY 14850, USA*
[2] *Kavli Institute at Cornell, Ithaca, NY 14853, USA*
(Dated: August 3, 2021)

Using a multilayer structure containing (cobalt detector layer)/(copper spacer)/(Permalloy source layer), we show experimentally how the non-reorientable spin-orbit torque generated by the Permalloy source layer – the component of spin-orbit torque that does not change when the Permalloy magnetization is rotated – can be measured using spin-torque ferromagnetic resonance (ST-FMR) with lineshape analysis. We find that dynamic spin pumping between the magnetic layers exerts torques on the magnetic layers as large or larger than the spin-orbit torques, so that if dynamic spin pumping is neglected the result would be a large overestimate of the spin-orbit torque. Nevertheless, the two effects can be separated by performing ST-FMR as a function of frequency. We measure a non-reorientable spin torque ratio $\xi_{\mathrm{DL}} = 0.04 \pm 0.01$ for spin current flow from Permalloy through an 8 nm Cu spacer to the Co, and a strength of dynamic spin pumping that is consistent with previous measurements by conventional ferromagnetic resonance.

I. INTRODUCTION

Current-induced spin-orbit torques offer the potential for efficient manipulation of nanoscale magnets for memory applications [1–3]. Among the families of materials that are of interest as potential sources of spin-orbit torque are metallic ferromagnets [4–19]. They are predicted to generate current-induced spin currents with both a reorientable component in which the spin is always parallel to the source-layer magnetization, plus a non-reorientable component (with a fixed spin direction in-plane and perpendicular to the charge current) that, remarkably, is not dephased within the source magnet even though the spin is not aligned with the magnetization [14]. The non-reorientable component has the same symmetries as the torque generated by the spin Hall effect from a non-magnetic source material.

Previously, spin-orbit torques from metallic ferromagnets have been probed indirectly by exciting nonlocal spin currents through magnetic insulators [10, 20–23], and the reciprocal process of spin-to-charge conversion has been measured for spin currents injected from an insulating ferromagnetic into a metallic ferromagnet [24–29]. However, it is more challenging to make direct measurements of spin-orbit torques generated by ferromagnets in magnetic trilayer structures that would be necessary for memory applications (i.e., ferromagnetic spin-source layer / non-magnetic spacer / ferromagnetic free layer to be manipulated). Ideally, one would like to apply a current and make quantitative measurements of just the deflection amplitude of the free-layer magnetization. However, in structures with two magnetic layers an applied current will exert torques on both layers and their dynamics will also be coupled by interlayer interactions, making it challenging to isolate just the strength of the spin-orbit torque acting on the free layer. For the reorientable component of the spin torque, one approach to address this challenge is to perform spin-torque ferromagnetic resonance (ST-FMR) experiments and analyze the dependence on dc current of the separate linewidths for each magnetic layer [7, 11, 15, 17–19], although care should be taken in avoiding artifacts that can affect this method [30, 31]. Here, we demonstrate that ST-FMR can also be used to achieve quantitative measurements of the non-reorientable (independent of the source-layer magnetization) component of spin-orbit torque generated by a ferromagnetic metal layer in a magnetic trilayer, by analyzing the resonant amplitudes and lineshapes. For a correct analysis of trilayers containing two metallic magnets (e.g., Co and Permalloy (Py)), it is critical to take into account that dynamic spin pumping [32, 33] couples the two magnetic layers and alters their resonance amplitudes. Still, the effects of spin currents associated with spin-orbit torques and those arising from dynamic spin pumping can be separated by analyzing the frequency dependence of the ST-FMR signals. Therefore, ST-FMR performed on magnetic trilayers can provide quantitative measurements of both the non-reorientable spin-orbit torque produced by a magnetic source layer and dynamic spin pumping. Our approach is similar to that of Yang et al. [34], except that their method does not account for dynamic spin pumping.

II. SAMPLE FABRICATION AND MEASUREMENTS

We used DC magnetron sputtering to grow our heterostructures onto thermally oxidized high-resistivity silicon wafers. Our heterostructures consisted of a Co "detector" layer, whose resonance dynamics we analyze, and a $Ni_{81}Fe_{19}$ (Py) "source" layer that generates a spin current to act on the Co. Specifically, the sample layer structure is SiO_x/Ta (1)/Cu (8)/Co (8)/Cu (8)/Py (t_{Py})/Ta (1) with numbers in parentheses indicating thickness in nm. The two Cu spacer layers have the same thickness, and are designed so that the in-plane component of the Oersted field that they generate will cancel within the Co detector, and consequently the only

net in-plane Oersted field acting on the Co layer will be due to current flowing within the Py layer. This will simplify our analysis of the spin-orbit torque acting on the Co layer. Cu was chosen for the spacer layers because of its long spin diffusion length and negligible spin Hall effect [35]. The Ta layers provide layer-smoothing and protection against oxidation, and have sufficiently large resistivity that they carry negligible current.

During the measurement, we apply an RF current together with an in-plane external magnetic field at an angle ϕ relative to the axis of current flow, and sweep the external field strength to tune through the magnetic resonance (Figure 1(b)). Each sample is studied using several different RF frequencies and field angles ϕ, and all measurements are performed at room temperature. We detect a DC signal that arises from mixing between the applied RF current and the resistance variations due to the angle-dependent magnetoresistance in both magnetic layers, originating from both anisotropic magnetoresistance within the layers and spin Hall magnetoresistance [36]. (We work at sufficiently large applied magnetic fields that the magnetizations of the Co and Py layers are saturated parallel in equilibrium, so contributions from giant magnetoresistance are second order in the precession angles, and negligible for the measurement.) The circuitry of the measurement is described elsewhere [37–39]. The two magnetic layers produce two resonances, with the lower resonant field being primarily from the Co and the higher resonant field primarily from the Py. We fit these resonances to two sets of symmetric and antisymmetric lorentzians.

The dependence on the angle ϕ for the symmetric and antisymmetric amplitudes of the (detector) Co-dominated resonance are shown in Figure 1(c) and (d): both follow a $\sin(2\phi)\cos(\phi)$ dependence. This is the form expected from "conventional" current-induced torques – from the in-plane component of the Oersted field and from spin-orbit torques arising from a spin current with polarization in-plane and perpendicular to the current. It is also the form expected in our geometry for torques arising from interfacial spin rotation as discussed in refs. [6, 8], and based on the analysis below the same angular dependence will be produced by the torques from dynamic spin pumping. We observe no significant contribution from unconventional current-induced torques that would lead to an altered angular dependence [40]. We note, however, that since both magnetizations have the same equilibrium orientation for our geometry, our measurements are not sensitive to the reorientable torques arising from the spin anomalous Hall effect or planar Hall effect [4, 11] which create spin currents whose polarization is parallel to the magnetization.

III. ANALYSIS: EFFECT OF DYNAMIC SPIN PUMPING

We can account for the resonant dynamics of the magnetic layers, including the effects of spin pumping between the layers, using a modified Landau-Lifshitz-Gilbert-Slonczewski (LLGS) equation [32, 33]

$$\dot{\mathbf{m}}_i = \alpha_i \mathbf{m}_i \times \dot{\mathbf{m}}_i + \boldsymbol{\tau}_{\mathrm{neq},i} + \boldsymbol{\tau}_{\mathrm{eq},i} - \alpha_i' \mathbf{m}_j \times \dot{\mathbf{m}}_j \quad (1)$$

where i and j identify the magnetic layers, $\boldsymbol{\tau}_{\mathrm{eq},i}$ are the equilibrium torques acting on layer i coming from the applied field and anisotropy, and $\boldsymbol{\tau}_{\mathrm{neq},i}$ are the non-equilibrium torques acting on layer i coming from spin-orbit torques and current-generated Oersted fields. α_i is the effective Gilbert damping parameter for layer i, including both the intrinsic damping and the time-averaged effect of the dynamically-pumped spins emerging from layer i, while the term containing α_i' describes the effect of the dynamically-pumped spins from layer j impinging on layer i to exert a time-dependent torque. Bilinear coupling of the form $\mathbf{m}_i \cdot \mathbf{m}_j$, which could arise from dipole or RKKY coupling [41], is generally also relevant in systems with more than one ferromagnetic layer, but we designed our Cu spacers to be sufficiently thick to minimize this effect, and found by measuring the shift of the minor loop in hysteresis measurements that it is indeed negligible in our system [42]. When a direct charge current flows perpendicular to the layers, spin-transfer torque can also provide additional interlayer coupling [43], but this effect is not relevant for our sample geometry.

Our treatment of the torques due to dynamic spin pumping follow references [32, 33, 44]. Compared to the more-familiar time-averaged DC component of the spin-pumped spin current that generates DC voltage signals in inverse spin Hall experiments [45–47] and modifies the magnetic damping [48, 49], the time-varying spin current associated with dynamic spin pumping is much larger. In systems with just a single ferromagnetic layer the effects from the dynamic portion of the pumped spins are generally time-averaged to zero, but with a second ferromagnetic layer present the pumped spins will induce dynamic coupling between the magnetic layers [32, 33, 50, 51]. Because the spins pumped by layer j are oscillating and are generally out-of-phase with the precession in layer i, they exert a nontrivial torque on layer i which depends on the phase difference between the oscillations of the two layers, introducing field and frequency dependence to the interaction. Based on this field and frequency dependence, we will show that it is possible to separate the effects of the spin-pumping-induced interaction between the layers from the direct effects of the non-reorientable spin-orbit torque from the source layer.

To model the resonance lineshapes, we consider the case that the resonance field is much larger than the coercive fields of both magnetic layers so that the equilibrium magnetizations of both layers are saturated in the same direction. We then solve for in-plane (x) and out-of-plane (z) magnetization deflection amplitudes of each layer (Fig. 1(a)), and only keep terms to first order in these deflections from equilibrium. We can find the magnetization deflection amplitudes of each layer by solving Eq. (1) following the same procedure as [52], noting that we can think of the dynamic spin pumping as

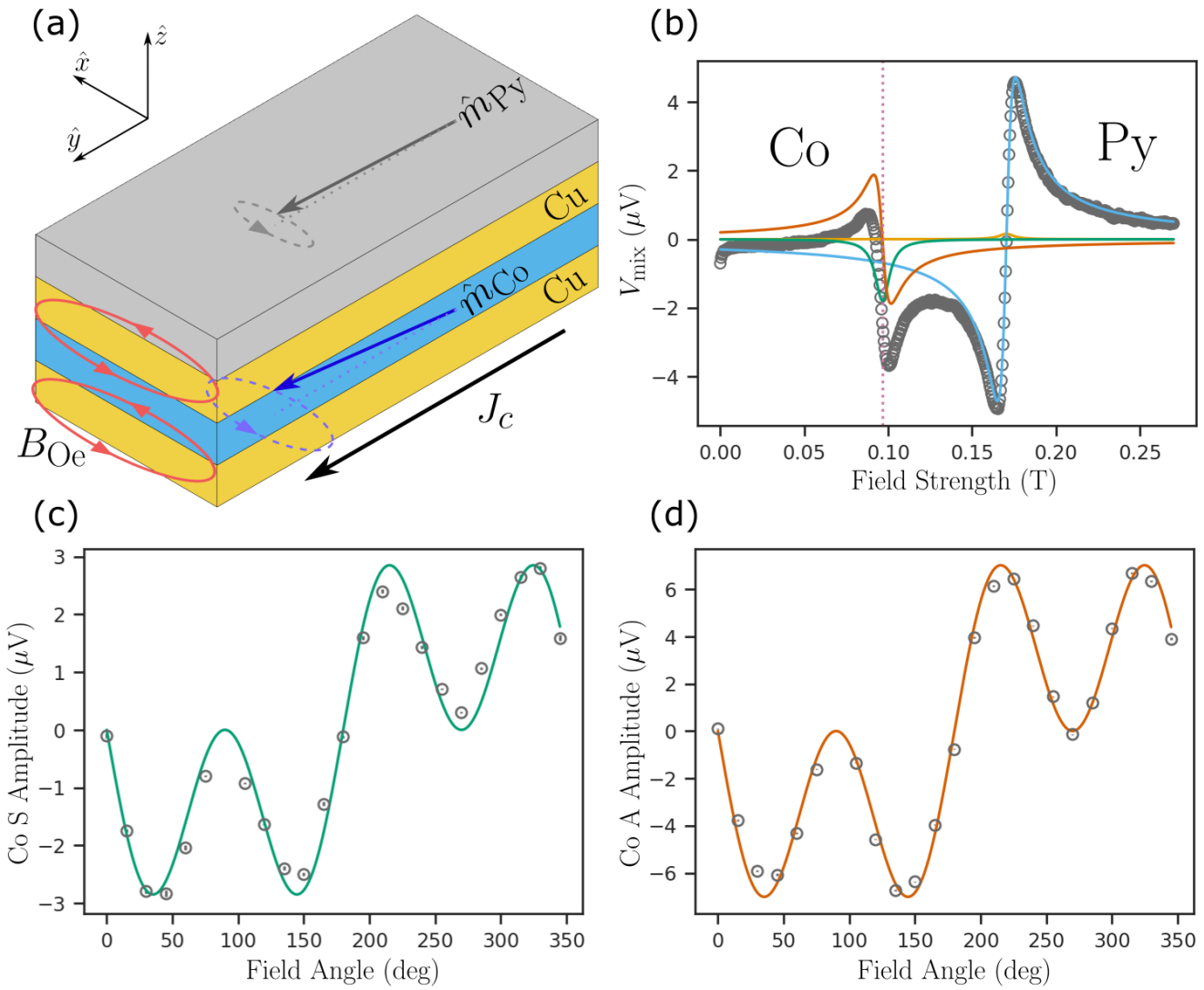

FIG. 1. (a) Schematic of the device, with a depiction of the magnetization oscillations near the Co-dominated resonance. The Oersted field from the symmetric spacer layers around the Co will cancel inside of the Co layer. Even at the Co-dominated resonance condition the amplitude of the Py-dominated mode is still significant. (b) Example resonance signal of the $t_{\mathrm{Py}} = 5.7$ nm sample showing the Co (left, lower resonant field) and Py (right, higher resonant field) dominated resonances and their symmetric and antisymmetric components for an applied microwave frequency $f = 8$ GHz. The dashed vertical line represents the Co-dominated resonance field. The antisymmetric part of the Py-dominated resonance is still substantial there. (c,d) The angular variation in the (c) symmetric and (d) antisymmetric components of the Co-dominated resonance, showing the $\sin(2\phi)\cos(\phi)$ angular dependence expected from SHE-like torques and in-plane Oersted torques, respectively.

effectively modifying the torques on each layer. The general solution for this system of two oscillators are normal modes which are linear combinations of the deflections of both layers. However, we will see that for our samples the layers are sufficiently weakly coupled that the oscillation amplitude of each normal mode is still dominated by only one magnet, and the two eigenfrequencies map to the resonant frequencies of the Co and Py individually, as given by the Kittel relation. The solution of Eq. (1) for the in-plane and out-of-plane magnetization deflection amplitudes of the detector layer are

$$m_{dx} = L_d\left(-\omega_{d2}\left[\tau_{dz} - i\omega\alpha'_d m_{sx}\right] + i\omega\left[\tau_{dx} + i\omega\alpha'_d m_{sz}\right]\right) \quad (2)$$

$$m_{dz} = L_d\left(\omega_{d1}\left[\tau_{dx} + i\omega\alpha'_d m_{sz}\right] + i\omega\left[\tau_{dz} + i\omega\alpha'_d m_{sx}\right]\right) \quad (3)$$

where the d subscript denotes parameters associated with the detection layer, $L_d = \left[\left(\omega^2 - \omega_{d0}^2\right) + i\omega\omega_d^+\alpha_d\right]^{-1}$, τ_{dx} and τ_{dz} the in-plane and out-of-plane non-equilibrium torques, $\omega_{d1} = \gamma B$, $\omega_{d2} = \gamma(B + \mu_0 M_{\mathrm{eff},d})$, $\omega_{d0}^2 = \omega_{d1}\omega_{d2}$, $\omega_d^+ = \omega_{d1} + \omega_{d2}$, and $\mu_0 M_{\mathrm{eff},d} = 1.82 \pm 0.09$ T for the Co layer which

was measured by measuring the resonance field as a function of the excitation frequency. The expressions for the source-layer deflections are the same as the detector layer's but with s and d interchanged and with $\mu_0 M_{\mathrm{eff},s} = 0.93 \pm 0.05$ T for the Py.

We can then completely decouple this system by ignoring any terms which are above first order in the α's and α''s. The result for the in-plane deflection amplitude of the detector layer, which generates the signal we are primarily concerned with, is

$$\begin{aligned} m_{dx} = L_d \{ & -\omega_{d2}\tau_{dz} + \overline{L}_s \alpha'_d \left[(\omega_{s0}^2 - \omega^2)(\omega_{s1} + \omega_{d2})\omega^2 \tau_{sx} - \omega^2 \omega_s^+ \alpha_s (\omega_{s2}\omega_{d2} + \omega^2)\tau_{sz} \right] \\ & + i\omega \left(\tau_{dx} + \overline{L}_s \alpha'_d \left[(\omega_{s0}^2 - \omega^2)(\omega_{s2}\omega_{d2} + \omega^2)\tau_{sz} + \omega^2 \omega_s^+ \alpha_s (\omega_{s1} + \omega_{d2})\tau_{sx} \right] \right) \} \end{aligned} \tag{4}$$

with $\overline{L}_s = \left[(\omega^2 - \omega_{s0}^2)^2 + \omega^2 \omega_s^{+2} \alpha_s^2 \right]^{-1}$ and $\omega_i^+ = \omega_{i1} + \omega_{i2}$. The real part of the expression within the curly braces corresponds to the antisymmetric component of the detector-layer-dominated resonance, with a lineshape of the form $(\omega^2 - \omega_{d0}^2)/\left[(\omega^2 - \omega_{d0}^2)^2 + \omega^2 \omega_d^{+2} \alpha_d^2 \right]$, and the imaginary part to the symmetric component, with a lineshape of the form $\omega^2 \omega_d^+ \alpha_d / \left[(\omega^2 - \omega_{d0}^2)^2 + \omega^2 \omega_d^{+2} \alpha_d^2 \right]$. The terms proportional to $\overline{L}_s \alpha'_d$ represent modifications of the usual expression for the ST-FMR resonance caused by spin pumping from the source layer. Through these terms, torques acting on the source layer (τ_{sx}, τ_{sz}) produce a modification of the torques acting on the detector layer, with the strength of the effect depending on the amplitude of the source-layer-dominated resonance through the frequency-dependent term $\overline{L}_s$. The source-layer-dominated resonance amplitude also includes symmetric and antisymmetric components. The terms inside of the square brackets which include $(\omega_{s0}^2 - \omega^2)$ correspond to the antisymmetric component of the source-layer-dominated resonance amplitude. The other components correspond to the symmetric component amplitude.

This expression can be simplified significantly for application to our measurements. First, since symmetric Lorentzians fall off quickly away from resonance and our resonances are always separated by at least six linewidths, the symmetric part of our (Py) source-layer-dominated resonance is essentially zero near the (Co) detector-layer-dominated resonance field as seen in Figure 1(b), so we can ignore all terms in Eq. (4) which correspond to the symmetric part of the source-dominated resonance. Second, the dampinglike torque acting on the source layer, τ_{sx}, is quite small compared to the Oersted torque on the detector layer, τ_{dz}, as illustrated in Figure 1(b) by the fact that the symmetric part of the Py-dominated resonance near the Py resonance field is small, as this is proportional to τ_{sx}. This allows us to ignore all terms in Eq. (4) which include τ_{sx} as well. After these simplifications, the in-plane deflection amplitude of the detector layer takes the form

$$\begin{aligned} m_{dx} = L_d \, & (-\omega_{d2}\tau_{dz} \\ & + i\omega \left(\tau_{dx} + \overline{L}_s \alpha'_d (\omega_{s0}^2 - \omega^2)(\omega_{s2}\omega_{d2} + \omega^2)\tau_{sz} \right)). \end{aligned} \tag{5}$$

The amplitude of the DC mixing signal we detect takes the more-tractable form

$$V_{\mathrm{mix}} = \frac{I}{2} \left(R_d^{\mathrm{AMR}} \, \mathrm{Re}\left[m_{dx} \right] + R_s^{\mathrm{AMR}} \, \mathrm{Re}\left[m_{sx} \right] \right) \sin(2\phi), \tag{6}$$

where I is the total current flowing in the multilayer and $R_i^{\mathrm{AMR}} \sin(2\phi)$ is the ϕ-derivative of the resistance change of the whole heterostructure due to the angle-dependent magnetoresistance of layer i. In general, it is also necessary to include an additional voltage signal due the DC component of the pumped spin current and the inverse spin Hall effect [45–47], but we calculate that this contribution is negligible for our samples (see Appendix A).

Even at the position of the detector-layer-dominated resonance it is not correct to ignore the contribution proportional to the source-layer magnetoresistance (the second term in Eq. (6)), because precession of the detector layer will produce dynamic spin pumping that drives precession of the source layer. Since this precession of the source layer is driven by spin pumping from the detector layer, near the detector layer's resonance condition the source-layer precession has the same resonant field and linewidth as the detector-layer resonance. This means that when we measure the lineshape which we attribute to the detector layer, some of this signal is actually due to the source-layer precession and the mixing voltage which results.

We can take into account the source-layer oscillations by writing their in-plane component in the form

$$\begin{aligned} m_{sx} = & L_s(-\omega_{s2}\tau_{sz} + i\omega\tau_{sx}) \\ & + L_d \overline{L}_s (\omega_{s0}^2 - \omega^2) \left[\omega^2 (\omega_{d1} + \omega_{s2})\tau_{dx}\alpha'_s \right. \\ & \left. + i\omega(\omega_{d2}\omega_{s2} + \omega^2)\tau_{dz}\alpha'_s \right] \end{aligned} \tag{7}$$

where the first term is the source-layer resonance in the absence of any dynamic spin pumping coupling and the L_d term is the one producing a resonance in the source layer of the same shape as the detector layer. Near the detector-layer resonance condition, the first term is essentially constant and hence will not play a significant role in our analysis.

Combining Eqs. (5), (6) and (7), the voltage amplitudes we measure upon fitting the detector-layer-dominated resonance as a sum of symmetric and antisymmetric Lorentzians is

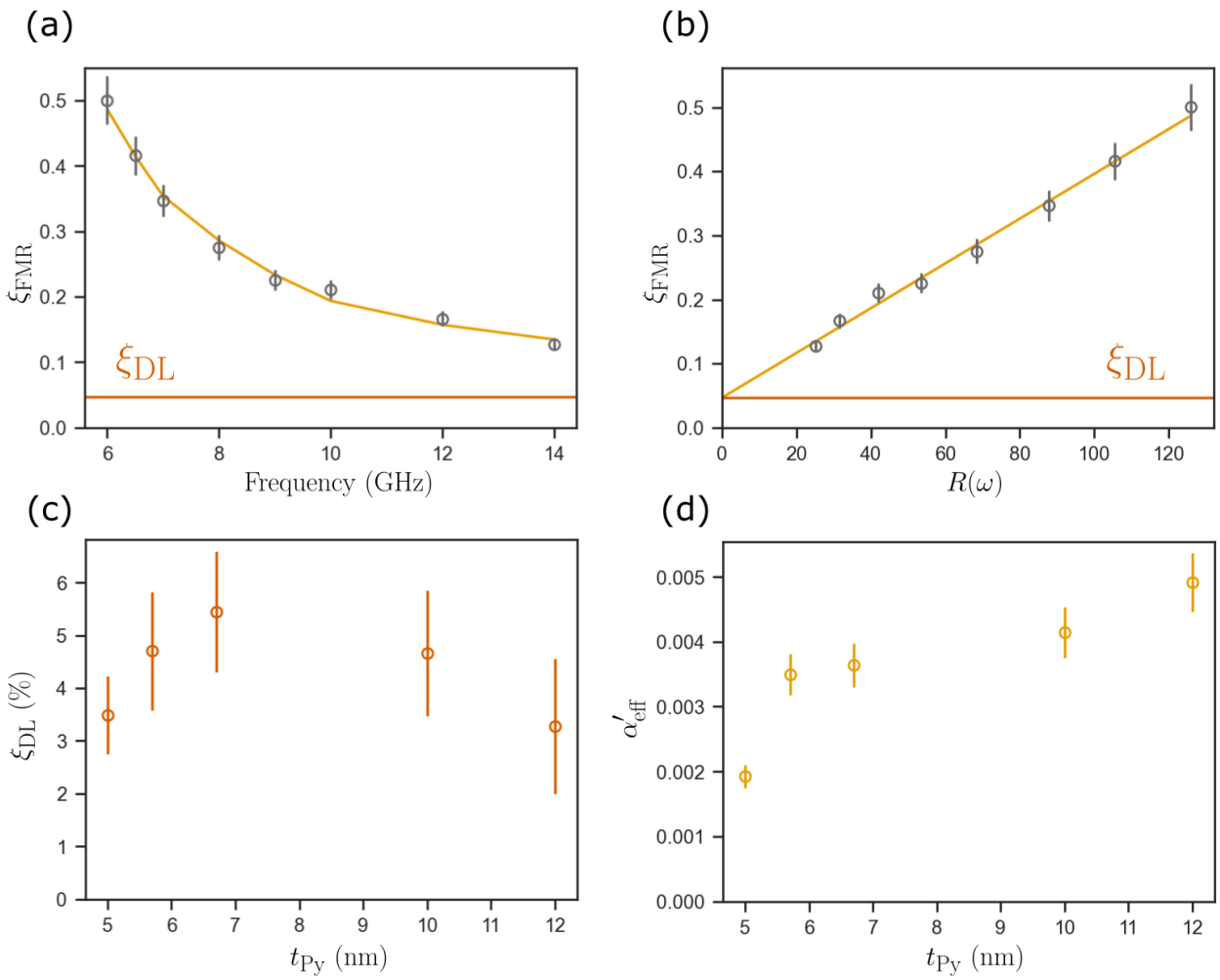

FIG. 2. (a,b) Measured values of ξ_{FMR} for a sample with 5.7 nm Py with a fit to Eq. (12). In (a) we plot the data versus frequency and in (b) we plot the same data versus calculated values of $R(\omega)$ to show that the data vary linearly with $R(\omega)$. The horizontal line is the extracted value of ξ_{DL}, which is the asymptote of (a) and the intercept of (b). (c) The effect of Py thickness on ξ_{DL}. (d) The dependence of the dynamic spin pumping parameter on the source Py layer thickness.

$$V_{dS} = \frac{IR_d^{\mathrm{AMR}}\sin(2\phi)}{2}\frac{1}{\alpha_d\omega_d^+}\left[\tau_{dx} + \overline{L}_{sA}(\omega_{s2}\omega_{d2}+\omega^2)\tau_{sz}\alpha'_d\right] + \frac{IR_s^{\mathrm{AMR}}\sin(2\phi)}{2}\frac{1}{\alpha_d\omega_d^+}\overline{L}_{sA}(\omega_{s2}\omega_{d2}+\omega^2)\tau_{dz}\alpha'_s \quad (8)$$

$$V_{dA} = \frac{IR_d^{\mathrm{AMR}}\sin(2\phi)}{2}\frac{1}{\alpha_d\omega_d^+}\frac{\omega_{d2}}{\omega}\tau_{dz} \quad (9)$$

where $\overline{L}_{sA} = \overline{L}_s(\omega_{s0}^2 - \omega^2)$. The first part of each mixing voltage comes from the detector layer and the second part is due to the source layer. There is also a small contribution of the source-layer-dominated resonance to V_{dA} that is not included in Eq. (9) because it contributes no more than 1 % of signal from the detector layer for our system, so we can ignore it in our analysis.

We are left with two significant modifications to the ST-FMR signals caused by dynamic spin pumping, both of which modify the measured symmetric lineshape amplitude of the detector-dominated resonance. The first is due to spins pumped from the source layer to the detector layer, thereby altering the detector-layer precession, an effect which is proportional to the Oersted torque on the source layer, τ_{sz}, with an amplitude proportional to the antisymmetric component of the source-layer-dominated resonance. This contribution adds directly to the dampinglike torque on the detector layer, τ_{dx}. The

second is due to spins pumped from the detector layer to the source layer, causing the source layer to oscillate with the same general lineshape as the detector-layer precession. The size of this term is proportional to the Oersted torque on the detector layer τ_{dz}, and it also has an amplitude proportional to the antisymmetric component of the source-layer resonance. From Eqs. (8) and (9) it is clear that the spin-pumping terms are not expected to alter the usual angular dependence of the ST-FMR signals ($\propto \sin(2\phi)\cos(\phi)$) as long as the current-induced torques are proportional to $\cos(\phi)$, the dependence expected for both conventional-symmetry spin-orbit torques and Oersted torques [40].

The efficiency of the antidamping spin-orbit torque generated by the Py source layer acting on the Co detector layer can be characterized by the antidamping torque efficiency, defined as

$$\xi_{\rm DL} = \tau_{dx}\frac{eM_{\rm sat,d}t_d}{\mu_B J_{c,s}}, \tag{10}$$

where e is the electron charge, $M_{{\rm sat},d} = 1.19 \pm 0.08 \times 10^6$ A/m for the Co layer, $t_d = 8$ nm for the Co layer, and $J_{c,s}$ the charge current density within the source magnetic layer. This efficiency, and also the influence of the dynamic spin pumping, can be determined by analyzing how the ratio of the symmetric and antisymmetric resonance amplitudes depends on measurement frequency. Following ref. [53], we first define an intermediate parameter

$$\xi_{\rm FMR} = \frac{e\mu_0 M_{{\rm sat},d}t_s t_d}{\hbar}\sqrt{\frac{\omega_{d2}}{\omega_{d1}}}\frac{V_{dS}}{V_{dA}} \tag{11}$$

where $t_s = t_{\rm Py}$. The values of $\xi_{\rm FMR}$ extracted for a sample with $t_s = 5.7$ nm as a function of different applied RF frequencies are shown by the circles in Figure 2(a). We find that $\xi_{\rm FMR}$ increases by more than a factor of 3 as the frequency is decreased from 14 GHz to 6 GHz, a much stronger dependence than is found in samples with nonmagnetic source layers [37]. We will show that this can be explained by dynamic spin pumping, in that for lower RF frequencies the resonance fields of the two magnetic layers move closer together, increasing the source layer resonance amplitude, and hence the value of $\overline{L}_{sA}$, at the detector-layer resonance condition which enhances the effects of the dynamic spin pumping.

For magnetic layers as thick as those we employ, $\geq$ 5 nm, and since the detector layer's interfaces are symmetric and are with the light metal Cu, Oersted torques should dominate over any weak interfacial field-like torques for both the source and detector layers [53–55]. We therefore assume that $\tau_{dz} = \gamma\mu_0 J_{c,s}t_s/2$ (only the current density within the source layer contributes to the Oersted field acting on the detector layer because the contributions from the Cu spacer layers cancel and the Ta layers have high resistivity and negligible current densities) and $\tau_{sz} = \gamma\mu_0(J_{c,d}t_d + J_{c,{\rm Cu}}t_{\rm Cu})/2$ (the current creating the Oersted field in the source layer comes from the detector layer and the Cu layers, which comprise the rest of the conductive layers in the device) [56, 57]. The ratio of these torques can be written $\tau_{sz}/\tau_{dz} = -(1-x_s)/x_s$ where x_s, the fraction of the total RF current flowing within the source layer, is in the range of 0.06 to 0.12 depending on the Py thickness and is calculated from the layer resistivities using a parallel-conduction model [58]. It then follows that

$$\xi_{\rm FMR} = \xi_{\rm DL} + R(\omega)\alpha'_{\rm eff} \tag{12}$$

with

$$R(\omega) = -\frac{e\mu_0 M_{{\rm sat},d}t_s t_d}{\hbar}\overline{L}_{sA}(\omega_{s2}\omega_{d2} + \omega^2)\frac{1-x_s}{x_s} \tag{13}$$

$$\alpha'_{\rm eff} = \alpha'_d - \frac{x_s}{1-x_s}\frac{R_s^{\rm AMR}}{R_d^{\rm AMR}}\alpha'_s. \tag{14}$$

All of the parameters that are frequency dependent are contained within $R(\omega)$, with the strongest frequency dependence coming from the term $\overline{L}_{sA}$ because it is sensitive to the separation of the the magnetic resonances. All of the parameters that enter $R(\omega)$ are independently measurable, so we can use Eq. (12) to fit to the data in Figure 2(a), using just two adjustable fit parameters, $\xi_{\rm DL}$ and $\alpha'_{\rm eff}$. The fit is shown both in Figure 2(a) and in Figure 2(b), which display the same data points plotted as a function of measurement frequency in (a) and as a function of $R(\omega)$ in (b). For the $t_{\rm Py} = 5.7$ nm sample, we find $\xi_{\rm DL} = 0.05 \pm 0.01$ and $\alpha'_{\rm eff} = 4.0 \pm 0.4 \times 10^{-3}$. The dominant source of uncertainty comes from the determination of $M_{{\rm eff},d}$ which we measure by fitting the frequency dependence of the detector-layer resonant field to the Kittel equation. We note in samples without dynamic spin pumping, and in which like our samples the field-like spin-orbit torque is negligible relative to the Oersted torque, $\xi_{\rm DL} = \xi_{\rm FMR}$. Therefore, Figure 2(a) illustrates that the neglect of spin-pumping in our analysis would lead to a large overestimate of $\xi_{\rm DL}$.

We have performed the same analysis on samples in which the Py layers vary in thickness from 5 nm to 12 nm. The results for $\xi_{\rm DL}$ and $\alpha'_{\rm eff}$ are shown in Figure 2(c) and (d). The overall dampinglike torque efficiency $\xi_{\rm DL}$ of the magnetization-independent spin-orbit torque from Py through the 8 nm Cu spacer to the Py layer is 0.04 ± 0.01, and it does not have a significant dependence on the Py thickness within our experimental uncertainty. The value we determine for $\alpha'_{\rm eff}$ does depend on the Py thickness, changing by more than a factor of 2 between Py thicknesses of 5 and 12 nm. The parameter α'_d should not depend on the Py thickness, so the changes in $\alpha'_{\rm eff}(t_{\rm Py})$ indicate that the second term in Eq. (14) is important as well as the first – that the signal at the detector-layer-dominated resonance is affected by spin pumping from the detector layer to the source layer that excites precession in the source (Py) layer. We are not able to make a separate determination of the parameters α'_d and α'_s in Eq. (14), however, because we are not able to make an accurate calibration of the ratio $R_s^{\rm AMR}/R_d^{\rm AMR}$. We can calibrate the anisotropic magnetoresistance of individual Co and Py layers, but

we find that when they are combined within a trilayer there is also a significant additional contribution from spin Hall magnetoresistance that cannot be calibrated without separate control over the magnetization angles in the two layers.

IV. DISCUSSION

We can compare our results to previous measurements. Efforts to determine the non-reorientable spin Hall effect in ferromagnetic layers via spin Seebeck and spin pumping experiments are complicated by difficulties in determining the interface spin mixing conductance [59] and the spin diffusion length. Furthermore, many of these experiments do not provide sufficient information to distinguish between the reorientable and non-reorientable components of the spin current generated by Py. The two measurements with direct quantitative claims we have found in this class of experiments give a value for the non-reorientable spin Hall ratio within Py of $\theta_{\rm SH}({\rm Py}) = 0.02$ by spin pumping in YIG/Cu/Py [25, 26]. The quantity we measure, the spin-orbit torque efficiency, $\xi_{\rm DL}$, is related to the spin Hall ratio as $\xi_{\rm DL} = \theta_{\rm SH}({\rm Py})T_{\rm int}$ where $T_{\rm int}$ is an interfacial spin transfer coefficient less than or equal to 1. Therefore our measurements establish a lower bound for the non-reorientable spin Hall effect for the Py in our samples, $\theta_{\rm SH}({\rm Py}) \geq 0.04 \pm 0.01$. We suspect the difference is that the spin mixing conductance may be overestimated [59] in refs. [25, 26], leading to an underestimate of $\theta_{\rm SH}({\rm Py})$. Miao et al. [24] and Wu et al. [27] studied YIG/Py samples and quoted values of $\theta_{\rm SH}({\rm Py})$ relative to values for similar samples made with Pt instead of Py: $\theta_{\rm SH}({\rm Py})/\theta_{\rm SH}({\rm Pt}) = 0.38$ [24] and 0.98 [27]. These estimates rely on assumptions that the interfacial spin transparency and spin diffusion lengths are similar for YIG/Py and YIG/Pt.

Das et al. [10, 20] detected both reorientable and non-reorientable components of spin-orbit torque generated by Py using nonlocal measurement scheme where a spin current generated in Py was converted to magnons in YIG which then were converted back into a spin current in Pt or Py and transduced into a voltage through the inverse spin Hall effect. Their value of $\theta_{\rm SH}({\rm Py})$ is only given in relation to that of Pt, they quote $[G_{\rm Py}\theta_{\rm SH}({\rm Py})]/[G_{\rm Pt}\theta_{\rm SH}({\rm Pt})] = 0.09$ where G_i is a parameter describing the spin current to magnon conversion in each of the materials. Yang et al. [34] attempted to measure the non-reorientable component of the spin curernt alone from Py using lineshape analysis of ST-FMR signals for Py/YIG and CoFeB/YIG samples (both with no spacer layer), but without accounting for dynamics spin pumping. They claimed values of the non-reorientable spin-orbit torque efficiencies $\xi_{\rm DL} = 0.009$ for Py acting on YIG and -0.0014 for CoFeB acting on YIG; values much lower in magnitude than our result. We suspect that these low values may be due primarily to poor interfacial spin transmission from the Py into the YIG. Low spin transparency has also been a general feature found in spin-orbit torque measurements from heavy metals acting on iron garnets (see the comparisons by Gupta et al. [60]).

Based on measurements of conventional FMR in magnet/spacer/magnet samples, the parameter $\alpha'_{\rm eff}$ is expected to have a scale comparable to the intrinsic Gilbert damping in magnetic layers, α [32]. This is true for our samples. The values of $\alpha'_{\rm eff}$ plotted in Fig. 2(d) are about half the damping parameters in our Co and Py layers determined by the ST-FMR fits.

V. CONCLUSION

We have measured and analyzed spin-torque ferromagnetic resonance (ST-FMR) signals for samples containing the layer structure Py source layer/Cu spacer/Co detector layer. We find that the resonance amplitudes and lineshapes are determined by a combination of direct current-induced torques and dynamic spin pumping between the magnetic layers. In fact, the strength of the torque created by dynamic spin pumping can be substantially larger than the direct current-induced spin-orbit torque, so the contribution from dynamic spin pumping should be considered whenever analyzing resonant measurements in samples with more than one ferromagnetic layer [13, 34]. The frequency dependence of the ST-FMR signals allows these two effects to be separated, and therefore our experiment provides independent measurements of the non-reorientable spin-orbit torque generated by the Py layer (the portion of the spin-orbit torque that does not depend on the orientation of the Py magnetization) and the strength of dynamical spin pumping. We find an efficiency for the non-reorientable spin-orbit torque generated by Py (and acting through a 8 nm Cu spacer) of 0.04 ± 0.01. The strength of the dynamic spin pumping, as characterized by the parameter $\alpha'_{\rm eff}$, appears consistent with previous measurements using conventional ferromagnetic resonance [32].

VI. ACKNOWLEDGEMENTS

We thank Bob Buhrman for discussions. This research was supported in part by Task 2776.047 of ASCENT, one of six centers in JUMP, a Semiconductor Research Corporation program sponsored by DARPA, and by the NSF (DMR-1708499). The devices were fabricated using the shared facilities of the Cornell NanoScale Facility, a member of the National Nanotechnology Coordinated Infrastructure (NNCI), and the Cornell Center for Materials Research, both of which are supported by the NSF (Grants No. NNCI-1542081 and No. DMR-1719875).

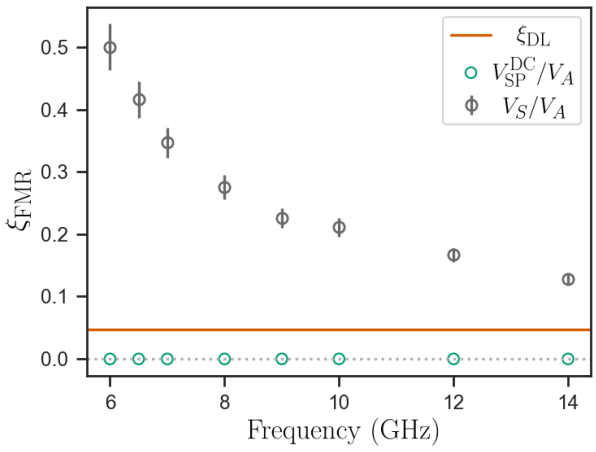

FIG. 3. Comparison of the DC spin pumping contribution to ξ_{FMR} to the total signal for 5.7 nm Py. The contribution is so small as to be negligible.

Appendix A: DC Spin Pumping Contribution

The DC component of the pumped spin current from the Co is converted into a DC charge current through the inverse spin Hall effect in the Py layer, as described in ref. [52]. The generated DC spin pumping voltage follows the form

$$V_{\mathrm{SP}}^{\mathrm{DC}} = -\frac{2e}{\hbar}\theta_{\mathrm{SH}} R_{\mathrm{tot}} W \sin\phi \frac{\hbar}{4\pi} g_{\mathrm{eff}}^{\uparrow\downarrow} \lambda_{\mathrm{sd,s}} \left[\frac{\omega_{d1}\tau_{dx}^2 + \omega_{d2}\tau_{dz}^2}{(\alpha_d \omega_d^+)^2} L_{dS}(B)\right] \tanh\left(\frac{t_s}{2\lambda_{sd,s}}\right) \tag{A1}$$

where R_{tot} is the total resistance of the heterostructure, W is the width of the device, $\lambda_{\mathrm{sd},s}$ is the spin diffusion length of the source, and $L_{dS}(B)$ is the symmetric lineshape of the detector layer. We have either measured or can estimate with reasonable certainty all quantities in this expression. For the $t_s = 5.7$ nm Py sample, $R_{\mathrm{tot}} = 12.1\,\Omega$, $W = 20\,\mu$m, $\alpha_d = 0.014$, $\theta_{\mathrm{SH}} \approx 0.05$, we approximate $g_{\mathrm{eff}}^{\uparrow\downarrow} \approx 8$ nm^{-2} [59] and $\lambda_{\mathrm{sd},s} \approx 10$ nm [61] as reasonable estimates compared to other systems, we approximate 1.5 mA of RF current is flowing in the Py layer using the input microwave power after accounting for loss in the cabling and current shunting, which leads to $\tau_{dx} \approx 4\times10^6$ s^{-1} and $\tau_{dz} \approx 8\times10^6$ s^{-1}, and ω_{d1}, ω_{d2} and ω_d^+, which are evaluated at the Co resonant field and hence depend on frequency, are on the order of 10 GHz, 300 GHz and 300 GHz, respectively. To compare this more directly to what we have measured before, we utilize the fact that this will only add to the symmetric component of the resonance. Since we look at the ratio of the symmetric and antisymmetric resonance amplitudes, we compute $V_{\mathrm{SP}}^{\mathrm{DC}}/V_A$ where V_A is the amplitude of the antisymmetric component of the Lorentzians. We then compare this to V_S/V_A in Figure 3, where we have included constants to convert the voltage ratios to torque efficiencies.

This contribution ends up being negligibly small, compared to both the total signal due to dynamic spin pumping and the signal due to the dampinglike torque from the source layer, never rising above 5 % of the measured symmetric signal for the thickest Py layers and at the highest frequencies but is less than 1 % for most thicknesses and frequencies. We therefore are justified in ignoring this contribution in our main analysis.

[1] A. Brataas, A. D. Kent, and H. Ohno, Current-induced torques in magnetic materials, Nature Materials **11**, 372 (2012).

[2] K. L. Wang, J. G. Alzate, and P. K. Amiri, Low-power non-volatile spintronic memory: STT-RAM and beyond, Journal of Physics D: Applied Physics **46**, 074003 (2013).

[3] F. Oboril, R. Bishnoi, M. Ebrahimi, and M. B. Tahoori, Evaluation of hybrid memory technologies using SOT-MRAM for on-chip cache hierarchy, IEEE Transactions on Computer-Aided Design of Integrated Circuits and Systems **34**, 367 (2015).

[4] T. Taniguchi, J. Grollier, and M. D. Stiles, Spin-transfer torques generated by the anomalous hall effect and anisotropic magnetoresistance, Physical Review Applied **3**, 044001 (2015).

[5] A. M. Humphries, T. Wang, E. R. J. Edwards, S. R. Allen, J. M. Shaw, H. T. Nembach, J. Q. Xiao, T. J. Silva, and X. Fan, Observation of spin-orbit effects with spin rotation symmetry, Nature Communications **8**, 911 (2017).

[6] V. P. Amin, J. Zemen, and M. D. Stiles, Interface-generated spin currents, Physical Review Letters **121**, 136805 (2018).

[7] S. Iihama, T. Taniguchi, K. Yakushiji, A. Fukushima, Y. Shiota, S. Tsunegi, R. Hiramatsu, S. Yuasa, Y. Suzuki, and H. Kubota, Spin-transfer torque induced

by the spin anomalous hall effect, Nature Electronics **1**, 120 (2018).

[8] S.-H. C. Baek, V. P. Amin, Y.-W. Oh, G. Go, S.-J. Lee, G.-H. Lee, K.-J. Kim, M. D. Stiles, B.-G. Park, and K.-J. Lee, Spin currents and spin–orbit torques in ferromagnetic trilayers, Nature Materials **17**, 509 (2018).

[9] J. D. Gibbons, D. MacNeill, R. A. Buhrman, and D. C. Ralph, Reorientable spin direction for spin current produced by the anomalous hall effect, Physical Review Applied **9**, 064033 (2018).

[10] K. S. Das, J. Liu, B. J. van Wees, and I. J. Vera-Marun, Efficient injection and detection of out-of-plane spins via the anomalous spin hall effect in permalloy nanowires, Nano Letters **18**, 5633 (2018).

[11] C. Safranski, E. A. Montoya, and I. N. Krivorotov, Spin–orbit torque driven by a planar hall current, Nature Nanotechnology **14**, 27 (2018).

[12] Y. Ou, Z. Wang, C. S. Chang, H. P. Nair, H. Paik, N. Reynolds, D. C. Ralph, D. A. Muller, D. G. Schlom, and R. A. Buhrman, Exceptionally high, strongly temperature dependent, spin hall conductivity of SrRuO3, Nano Letters **19**, 3663 (2019).

[13] M. W. Keller, K. S. Gerace, M. Arora, E. K. Delczeg-Czirjak, J. M. Shaw, and T. J. Silva, Near-unity spin hall ratio in Ni_xCu_{1-x} alloys, Physical Review B **99**, 214411 (2019).

[14] V. P. Amin, J. Li, M. D. Stiles, and P. M. Haney, Intrinsic spin currents in ferromagnets, Physical Review B **99**, 220405(R) (2019).

[15] T. Seki, S. Iihama, T. Taniguchi, and K. Takanashi, Large spin anomalous hall effect in L10-FePt : Symmetry and magnetization switching, Physical Review B **100**, 144427 (2019).

[16] T. Y. Ma, C. H. Wan, X. Wang, W. L. Yang, C. Y. Guo, C. Fang, M. K. Zhao, J. Dong, Y. Zhang, and X. F. Han, Evidence of magnetization switching by anomalous spin hall torque in NiFe, Physical Review B **101**, 134417 (2020).

[17] C. Safranski, J. Z. Sun, J.-W. Xu, and A. D. Kent, Planar hall driven torque in a ferromagnet/nonmagnet/ferromagnet system, Physical Review Letters **124**, 197204 (2020).

[18] Y. Hibino, K. Yakushiji, A. Fukushima, H. Kubota, and S. Yuasa, Spin-orbit torque generated from perpendicularly magnetized Co/Ni multilayers, Physical Review B **101**, 174441 (2020).

[19] Y. Koike, S. Iihama, and S. Mizukami, Composition dependence of the spin-anomalous hall effect in a ferromagnetic Fe–Co alloy, Japanese Journal of Applied Physics **59**, 090907 (2020).

[20] K. S. Das, W. Y. Schoemaker, B. J. van Wees, and I. J. Vera-Marun, Spin injection and detection via the anomalous spin hall effect of a ferromagnetic metal, Physical Review B **96**, 220408(R) (2017).

[21] J. Cramer, A. Ross, S. Jaiswal, L. Baldrati, R. Lebrun, and M. Kläui, Orientation-dependent direct and inverse spin hall effects in Co60Fe20B20, Physical Review B **99**, 104414 (2019).

[22] Y. Omori, E. Sagasta, Y. Niimi, M. Gradhand, L. E. Hueso, F. Casanova, and Y. C. Otani, Relation between spin hall effect and anomalous hall effect in 3d ferromagnetic metals, Physical Review B **99**, 014403 (2019).

[23] T. Wimmer, B. Coester, S. Geprägs, R. Gross, S. T. B. Goennenwein, H. Huebl, and M. Althammer, Anomalous spin hall angle of a metallic ferromagnet determined by a multiterminal spin injection/detection device, Applied Physics Letters **115**, 092404 (2019).

[24] B. F. Miao, S. Y. Huang, D. Qu, and C. L. Chien, Inverse spin hall effect in a ferromagnetic metal, Physical Review Letters **111**, 066602 (2013).

[25] H. Wang, C. Du, P. C. Hammel, and F. Yang, Spin current and inverse spin hall effect in ferromagnetic metals probed by Y3Fe5O12-based spin pumping, Applied Physics Letters **104**, 202405 (2014).

[26] C. Du, H. Wang, F. Yang, and P. C. Hammel, Systematic variation of spin-orbit coupling withd-orbital filling: Large inverse spin hall effect in 3d transition metals, Physical Review B **90**, 140407(R) (2014).

[27] H. Wu, C. H. Wan, Z. H. Yuan, X. Zhang, J. Jiang, Q. T. Zhang, Z. C. Wen, and X. F. Han, Observation of pure inverse spin hall effect in ferromagnetic metals via ferromagnetic/antiferromagnetic exchange-bias structures, Physical Review B **92**, 054404 (2015).

[28] M. Wahler, N. Homonnay, T. Richter, A. Mller, C. Eisenschmidt, B. Fuhrmann, and G. Schmidt, Inverse spin hall effect in a complex ferromagnetic oxide heterostructure, Scientific Reports **6**, 28727 (2016).

[29] D. Tian, Y. Li, D. Qu, S. Y. Huang, X. Jin, and C. L. Chien, Manipulation of pure spin current in ferromagnetic metals independent of magnetization, Physical Review B **94**, 020403(R) (2016).

[30] J.-W. Xu and A. D. Kent, Charge-to-spin conversion efficiency in ferromagnetic nanowires by spin torque ferromagnetic resonance: Reconciling lineshape and linewidth analysis methods, Physical Review Applied **14**, 014012 (2020).

[31] S. Karimeddiny and D. C. Ralph, Resolving discrepancies in spin-torque ferromagnetic resonance measurements: Lineshape versus linewidth analyses, Physical Review Applied **15**, 064017 (2021).

[32] B. Heinrich, Y. Tserkovnyak, G. Woltersdorf, A. Brataas, R. Urban, and G. E. W. Bauer, Dynamic exchange coupling in magnetic bilayers, Physical Review Letters **90**, 187601 (2003).

[33] Y. Pogoryelov, M. Pereiro, S. Jana, A. Kumar, S. Akansel, M. Ranjbar, D. Thonig, D. Primetzhofer, P. Svedlindh, J. Åkerman, O. Eriksson, O. Karis, and D. A. Arena, Nonreciprocal spin pumping damping in asymmetric magnetic trilayers, Physical Review B **101**, 054401 (2020).

[34] W. L. Yang, J. W. Wei, C. H. Wan, Y. W. Xing, Z. R. Yan, X. Wang, C. Fang, C. Y. Guo, G. Q. Yu, and X. F. Han, Determining spin-torque efficiency in ferromagnetic metals via spin-torque ferromagnetic resonance, Physical Review B **101**, 064412 (2020).

[35] J. Bass and W. P. Pratt, Spin-diffusion lengths in metals and alloys, and spin-flipping at metal/metal interfaces: an experimentalist's critical review, Journal of Physics: Condensed Matter **19**, 183201 (2007).

[36] H. Nakayama, M. Althammer, Y.-T. Chen, K. Uchida, Y. Kajiwara, D. Kikuchi, T. Ohtani, S. Geprägs, M. Opel, S. Takahashi, R. Gross, G. E. W. Bauer, S. T. B. Goennenwein, and E. Saitoh, Spin hall magnetoresistance induced by a nonequilibrium proximity effect, Physical Review Letters **110**, 206601 (2013).

[37] L. Liu, T. Moriyama, D. C. Ralph, and R. A. Buhrman, Spin-torque ferromagnetic resonance induced by the spin hall effect, Physical Review Letters **106**, 036601 (2011).

[38] C.-F. Pai, L. Liu, Y. Li, H. W. Tseng, D. C. Ralph, and R. A. Buhrman, Spin transfer torque devices utilizing

the giant spin hall effect of tungsten, Applied Physics Letters **101**, 122404 (2012).
[39] C. He, G. Yu, C. Grezes, J. Feng, Z. Zhao, S. A. Razavi, Q. Shao, A. Navabi, X. Li, Q. L. He, M. Li, J. Zhang, K. L. Wong, D. Wei, G. Zhang, X. Han, P. K. Amiri, and K. L. Wang, Spin-torque ferromagnetic resonance in W/Co-Fe-B/W/Co-Fe-B/MgO stacks, Physical Review Applied **10**, 034067 (2018).
[40] D. MacNeill, G. M. Stiehl, M. H. D. Guimaraes, R. A. Buhrman, J. Park, and D. C. Ralph, Control of spin–orbit torques through crystal symmetry in WTe2/ferromagnet bilayers, Nature Physics **13**, 300 (2016).
[41] F. Hellman, A. Hoffmann, Y. Tserkovnyak, G. S. D. Beach, E. E. Fullerton, C. Leighton, A. H. MacDonald, D. C. Ralph, D. A. Arena, H. A. Dürr, P. Fischer, J. Grollier, J. P. Heremans, T. Jungwirth, A. V. Kimel, B. Koopmans, I. N. Krivorotov, S. J. May, A. K. Petford-Long, J. M. Rondinelli, N. Samarth, I. K. Schuller, A. N. Slavin, M. D. Stiles, O. Tchernyshyov, A. Thiaville, and B. L. Zink, Interface-induced phenomena in magnetism, Reviews of Modern Physics **89**, 025006 (2017).
[42] See supplemental material at [url will be inserted by publisher] for details of minor loop hysteresis measurements.
[43] S. Urazhdin, Dynamical coupling between ferromagnets due to spin transfer torque: Analytical calculations and numerical simulations, Physical Review B **78**, 060405(R) (2008).
[44] Y. Tserkovnyak, A. Brataas, G. E. W. Bauer, and B. I. Halperin, Nonlocal magnetization dynamics in ferromagnetic heterostructures, Reviews of Modern Physics **77**, 1375 (2005).
[45] E. Saitoh, M. Ueda, H. Miyajima, and G. Tatara, Conversion of spin current into charge current at room temperature: Inverse spin-hall effect, Applied Physics Letters **88**, 182509 (2006).
[46] O. Mosendz, V. Vlaminck, J. E. Pearson, F. Y. Fradin, G. E. W. Bauer, S. D. Bader, and A. Hoffmann, Detection and quantification of inverse spin hall effect from spin pumping in permalloy/normal metal bilayers, Physical Review B **82**, 214403 (2010).
[47] A. Azevedo, L. H. Vilela-Leão, R. L. Rodríguez-Suárez, A. F. Lacerda Santos, and S. M. Rezende, Spin pumping and anisotropic magnetoresistance voltages in magnetic bilayers: Theory and experiment, Physical Review B **83**, 144402 (2011).
[48] Y. Tserkovnyak, A. Brataas, and G. E. W. Bauer, Enhanced gilbert damping in thin ferromagnetic films, Physical Review Letters **88**, 117601 (2002).
[49] S. Mizukami, Y. Ando, and T. Miyazaki, Magnetic relaxation of normal-metal (NM)/80NiFe/NM films, Journal of Magnetism and Magnetic Materials **239**, 42 (2002).
[50] D. Richardson, K. Srinivasan, A. Kalitsov, A. Ajan, S. Jain, S. Katz, and M. Wu, Interlayer exchange coupling in magnetic hard-soft bilayered structures, Physical Review Applied **11**, 044016 (2019).
[51] R. Medwal, S. Gupta, R. S. Rawat, A. Subramanian, and Y. Fukuma, Spin pumping in asymmetric Fe 50 Pt 50 /Cu/Fe 20 Ni 80 trilayer structure, physica status solidi (RRL) – Rapid Research Letters **13**, 1900267 (2019).
[52] S. Karimeddiny, J. A. Mittelstaedt, R. A. Buhrman, and D. C. Ralph, Transverse and longitudinal spin-torque ferromagnetic resonance for improved measurement of spin-orbit torque, Physical Review Applied **14**, 024024 (2020).
[53] C.-F. Pai, Y. Ou, L. H. Vilela-Leão, D. C. Ralph, and R. A. Buhrman, Dependence of the efficiency of spin hall torque on the transparency of Pt/ferromagnetic layer interfaces, Physical Review B **92**, 064426 (2015).
[54] I. M. Miron, K. Garello, G. Gaudin, P.-J. Zermatten, M. V. Costache, S. Auffret, S. Bandiera, B. Rodmacq, A. Schuhl, and P. Gambardella, Perpendicular switching of a single ferromagnetic layer induced by in-plane current injection, Nature **476**, 189 (2011).
[55] M. Jiang, H. Asahara, S. Sato, S. Ohya, and M. Tanaka, Suppression of the field-like torque for efficient magnetization switching in a spin–orbit ferromagnet, Nature Electronics **3**, 751 (2020).
[56] D. Gall, Electron mean free path in elemental metals, Journal of Applied Physics **119**, 085101 (2016).
[57] F. Warkusz, Size effects in metallic films, ElectroComponent Science and Technology **5**, 99 (1978).
[58] See supplemental material at [url will be inserted by publisher] for details on the parallel conduction model used to determine current shunting factors.
[59] L. Zhu, D. C. Ralph, and R. A. Buhrman, Effective spin-mixing conductance of heavy-metal–ferromagnet interfaces, Physical Review Letters **123**, 057203 (2019).
[60] V. Gupta, T. M. Cham, G. M. Stiehl, A. Bose, J. A. Mittelstaedt, K. Kang, S. Jiang, K. F. Mak, J. Shan, R. A. Buhrman, and D. C. Ralph, Manipulation of the van der waals magnet Cr2Ge2Te6 by spin–orbit torques, Nano Letters **20**, 7482 (2020).
[61] J. Bass, CPP magnetoresistance of magnetic multilayers: A critical review, Journal of Magnetism and Magnetic Materials **408**, 244 (2016).